

## Turbulence reduction by screens

By JOHAN GROTH AND ARNE V. JOHANSSON

Department of Mechanics, The Royal Institute of Technology, S-100 44 Stockholm, Sweden

(Received 13 April 1987 and in revised form 6 May 1988)

Turbulence suppression by use of screens was studied in a small wind tunnel especially designed and built for the purpose. Wide ranges of mesh sizes and wire-diameter Reynolds numbers were covered in the present investigation, enabling the study of sub- and super-critical screens under the same, well-controlled, flow conditions. For the latter type small-scale fluctuations, produced by the screen itself, interact with the incoming turbulence. In the immediate vicinity of the screen the turbulence was found to be highly anisotropic and the intensities were higher than on the upstream side. Downstream of a short initial decay region, where the intensities decrease rapidly, the return to isotropy was found to be much slower than for the unmanipulated turbulence. The latter was generated by a square rod grid, and was shown to become practically isotropic beyond a distance of roughly 20 mesh widths from the grid. The role of the turbulence scales for the overall reduction effectiveness, and for the optimization of screen combinations for application in low-turbulence wind tunnels was studied.

---

### 1. Introduction

The effects on turbulence of screens or wire gauzes is a classical topic for both theoretical and experimental turbulence investigations, as may be seen from the review material in Corrsin (1963) and Laws & Livesey (1978). The latter also deals with various other aspects of flow through screens, such as effects on mean velocity distributions and mean flow direction. In the present study we will focus on the turbulence reduction processes in the case of a uniform, perpendicularly oncoming stream with moderate turbulence intensities, which is a problem of considerable practical importance. For instance, the use of screens to improve flow quality in wind tunnels was first suggested by Prandtl (1932). Limitations on power input and cooling devices are factors that contribute to the importance of optimizing the use of screens for turbulence reduction at a given pressure drop.

The problem of turbulence suppression by screens also contains many interesting basic features of how turbulent eddies of disparate scales interact, etc. On the upstream side there is a pressure redistribution, and a stream contraction into the centre-plane of the screen, whereas on the downstream side thin shear layers are present and vortices are shed if the Reynolds number ( $Re_a$ ) based on wire diameter is large enough ( $\gtrsim 40$ ). The processes may be expected to be quite different above and below this value of the Reynolds number, which hence is one of the primary parameters to characterize the effects of a screen. Another parameter that influences the pressure drop across the screen is the solidity,  $\sigma$ , defined as projected solid area per unit total area. For values of  $\sigma$  higher than about 0.5 flow instabilities due to jet coalescence may occur (see e.g. Baines & Peterson 1951). Screens for turbulence

suppression, hence, always have solidities below this value. The change in flow direction can be described by a refraction coefficient,  $\alpha$  (see e.g. Laws & Livesey 1978), defined as the ratio between the flow angles on the downstream and upstream sides, respectively.

A complete theoretical treatment of the flow through a screen is, as yet, not a tractable problem, but various theoretical modelling efforts have been made. Taylor & Batchelor (1949) studied the effect of screens both on steady mean flow disturbances and on turbulence by a linear, inviscid analysis, neglecting the generation of turbulence by the screen itself (see also Batchelor 1976). Assuming isotropy for the incoming turbulence, they could determine reduction factors for the streamwise and lateral intensities, which depend solely on  $\alpha$  and the static pressure drop coefficient for the screen.

Dryden & Schubauer (1947) put forward a simple empirical formula for the reduction factors. The bulk of their experiments were carried out with the screens placed in the settling chamber of a wind tunnel, while the actual measurements were made in the test section. They noted that for a given total pressure drop it is advantageous to use several screens with relatively low pressure drop coefficients. Schubauer, Spangenberg & Klebanoff (1950) studied damping characteristics of screens both in the super- and the sub-critical ranges. They also investigated the dependence of the critical Reynolds number on solidity in the range 0.19–0.57. Several experimental investigations of turbulence reduction by screens and other flow manipulators have been carried out by Nagib and coworkers. Tan-Atichat, Nagib & Loehrke (1982) studied the effects of screens and perforated plates on the streamwise turbulence intensity in two small wind tunnels (diameters 7 and 15 cm), for a variety of incoming flow conditions. They found that for supercritical screens the mesh size should be chosen such that the lengthscales of the turbulence generated by the screen are smaller than those of the incoming turbulence, but not much smaller. The motivation given for this was that under these conditions the spectral transfer of energy to dissipative scales would be maximized.

Turbulence was, in the present study, generated by means of a square rod grid, and wide ranges of the screen mesh size and Reynolds number,  $Re_d$ , were covered. Subcritical screens ( $Re_d < 40$ ) were shown to give a large reduction, but the maximum turbulence suppression for a given total pressure drop was found for cascade type of combinations in which the screen furthest downstream has a low supercritical Reynolds number, whereas the upstream ones are chosen to be relatively coarse. However, the mesh width should be significantly smaller than the typical scale of the incoming turbulence. Very few data exist in the literature regarding the behaviour of the lateral turbulence intensities behind screens. In the present study the manner in which the flow behind screens, as well as grids, returns to isotropy was studied.

## **2. Experimental apparatus and procedure**

The present flow facility was designed specifically for the study of turbulence damping by screens and permits different screens and screen combinations to be readily interchanged. It is built as an open-circuit blowing type wind tunnel with a 2 m long ( $0.45 \times 0.45 \text{ m}^2$ ) test section. Mufflers were placed on both sides of the fan to obtain a low noise level. The fan motor was equipped with guide vanes to reduce swirl and a conical afterbody long enough to prevent separation. Two honeycombs and

No.	Meshes (in. <sup>-1</sup> )	Wire diameter (mm)	Solidity	$Re_d$	$K$
1	2.1	2.50	0.37	830	0.68
2	4.9	1.00	0.35	330	0.66
3	7.9	0.50	0.29	170	0.49
4	12.1	0.50	0.42	170	0.99
5	19.0	0.24	0.33	80	0.79
6	34.0	0.19	0.44	65	1.64
7	147.0	0.04	0.41	13	2.90
Grid	1.0	6.00	0.42	2000	

TABLE 1. Basic data for the grid and the screens. Reynolds numbers and resistance coefficient ( $K$ ) values are given at a mean velocity of 5 m/s.

four screens eliminate to a high degree the remnants of swirl and other flow disturbances introduced by the fan.

Turbulence was generated by means of a biplane grid, made of wooden rods of square cross-section ( $6 \times 6 \text{ mm}^2$ ). The solidity was 0.42 and the mesh width 25 mm. For the bulk of the experiments presented here it was placed 20 mesh widths upstream of the position where the screens to be studied were inserted. This ensures that the screens will be far enough downstream to avoid the initial region of strong anisotropy, and that the turbulence has become laterally homogeneous (see e.g. Hinze 1959). Combinations with up to five screens were used here, but the set-up allows for practically any number of screens. The separations could be varied from 0.05 m to 0.30 m by means of inserts.

The flow behind the grid had a mean velocity ( $U$ ) of about 5 m/s, and was reasonably uniform in the streamwise direction and in cross-stream planes. The difference between the maximum and minimum velocity values within a streamtube  $0.1 \times 0.1 \text{ m}^2$  along the centreline of the test section was less than 4% of the mean velocity. Without grid or screens the turbulence level was approximately 0.4% at the beginning of the test section. The lateral dimension (0.45 m) was sufficiently large to ensure negligible influence from the wall boundary layers, and to provide a good homogeneity in the cross-stream direction of the grid turbulence. A zero pressure gradient, and hence constant free-stream velocity, was ensured by a slightly increasing cross-sectional area in the streamwise direction. This was achieved by giving one of the walls an opening angle of  $0.7^\circ$ .

The seven different types of screens used cover a wide range of mesh sizes and wire diameters (see table 1). The solidity was in all cases below 0.44 to avoid jet coalescence. The coarsest screen had a mesh size of half of that of the grid or 70 times that of the finest screen. The latter is subcritical at the velocities used here, its Reynolds number ( $Re_d$ ) based on the wire diameter being only about 10. For Reynolds numbers below roughly 40 no turbulence will be produced by vortex shedding. Schubauer *et al.* (1950) found a critical Reynolds number of about 50 for a solidity of 0.4. The present findings (figure 1) indicate that the transition from subcritical to supercritical behaviour is smooth in terms of the pressure drop.

The static pressure drop across a screen is, in wind-tunnel applications, the penalty to be weighed against the positive effect of turbulence reduction. A natural aim would hence be to maximize the damping for a given pressure drop. The dependence

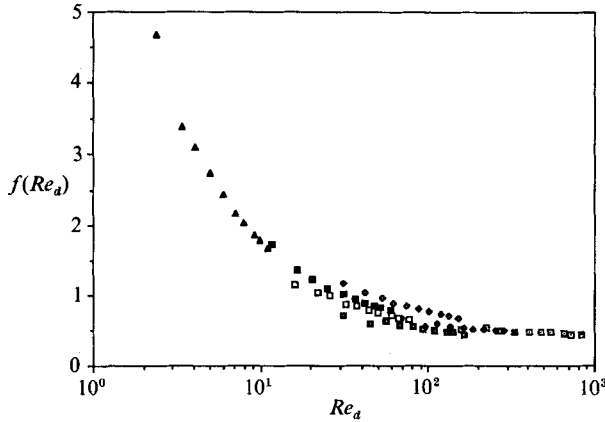


FIGURE 1. The static pressure drop function  $f$  as a function of the wire diameter Reynolds number. Data for all the seven screens at ten different velocities are included. Each screen is represented by a separate symbol.

of the static pressure drop coefficient,  $K$ , on the Reynolds number and the solidity,  $\sigma$ , can be expressed as (see Pinker & Herbert 1967 or Laws & Livesey 1978)

$$K \equiv \frac{\Delta p_{\text{stat}}}{0.5\rho U^2} = f(Re_d) \frac{1 - (1 - \sigma)^2}{(1 - \sigma)^2}, \quad (2.1)$$

where  $\rho$  is the fluid density and  $f(Re_d)$  is an empirical function. The function  $f(Re_d)$  can be seen in figure 1 to reach a constant value of about 0.45 for high  $Re_d$ -values, but increases quite dramatically with decreasing Reynolds numbers below 100. Hence, subcritical screens give a high static pressure drop coefficient. For a given screen the  $K$ -value is about three times larger at  $Re_d = 10$  as compared to that at  $Re_d = 100$ . Taylor & Davies (1944) made pressure drop measurements in the Reynolds number range 250–600. They found a trend that well agrees with that in figure 1 and their asymptotic pressure drop coefficient corresponds to  $f = 0.45$  for  $\sigma = 0.35$ . For higher solidities, however, their asymptotic values are higher (up to 0.6). Pinker & Herbert (1967) present pressure drop data for Reynolds numbers above 300 with  $\sigma$  in the range 0.36–0.68. Their  $f$ -values decrease slightly with Reynolds number and level off at about 0.50, which is somewhat higher than the value found here. It is noteworthy that the data in figure 1 cover Reynolds numbers all the way between 2 and 850.

The turbulence measurements were carried out with standard hot-wire single and X-probes, as well as a hot-film X-probe. These could be traversed in the streamwise direction (along the  $x$ -axis) and vertically (along the  $y$ -axis). The anemometer signals were sampled and stored with a MINC PDP 11/23 on which also all data evaluation was made.

In order to correctly evaluate the degree of anisotropy behind grids and screens it is essential, when using hot wires or hot films, to be aware of the influence of tangential cooling. This can be taken into account in two different ways, viz. either by calibrating the probes against flow velocity and angle or by using the complete cosine law including the tangential cooling coefficient  $k$ . For an X-probe in the  $(x, y)$ -plane with wires in  $45^\circ$  to the mean flow direction the effective cooling velocities can be expressed as

$$U_{\text{eff},2} = \left\{ \left( \frac{U + u \pm v}{\sqrt{2}} \right)^2 + k^2 \left( \frac{U + u \mp v}{\sqrt{2}} \right)^2 + k^2 w^2 \right\}^{\frac{1}{2}}, \quad (2.2)$$

where  $u$ ,  $v$  and  $w$  denote the velocity fluctuations in the streamwise ( $x$ ) and lateral ( $y$ ,  $z$ ) directions. The measured  $u$  and  $v$  components are calculated as  $U_{\text{eff}_1} \pm U_{\text{eff}_2}$ , respectively, divided by  $\sqrt{2}$  and a factor  $(1+k^2)^{\frac{1}{2}}$ , where the latter arises from the calibration procedure. This yields the following lowest-order relations between measured and true values of the turbulence intensities:

$$(u_{\text{rms}})_{\text{meas}} = u_{\text{rms}}, \quad (v_{\text{rms}})_{\text{meas}} = \frac{1-k^2}{1+k^2} v_{\text{rms}}. \quad (2.3)$$

The same correction as for  $v_{\text{rms}}$  is also valid for the mean value of  $uv$ . The  $k$ -value for hot wires was determined for various length to diameter ratios by Champagne, Sleicher & Wehrmann (1967). For  $l/d = 200$  (as used here) the  $k$ -value was found to be 0.2, which means that the measured  $v_{\text{rms}}$ -value is 8% too low if the tangential cooling is neglected. A cylindrical hot-film X-probe was found to give practically identical results as the hot wires when its tangential cooling sensitivity was accounted for. The hot-film (DISA 55R61)  $k$ -factor deduced from comparisons between the measured  $v_{\text{rms}}$ -values from the hot-film and hot-wire probes was 0.32. This agrees well with that (0.35) determined by Alfredsson & Johansson (unpublished results). The correction for the hot-film probe, hence, corresponds to 23% of the measured  $v_{\text{rms}}$ .

### 3. Results

The turbulence intensities (normalized by  $U$ ) produced by the grid were approximately 5.5% both in the streamwise and the lateral directions at  $x = 0$ , i.e. at 20 mesh widths ( $M$ ) downstream the grid. This is the position where screens are inserted and if only one is used,  $x$  is hence measured from that screen. It has been reported in several earlier investigations that turbulence behind a grid retains a small degree of anisotropy over very large downstream distances. For instance, Comte-Bellot & Corrsin (1966) found a practically constant value of  $v_{\text{rms}}/u_{\text{rms}}$  slightly above 0.9, over as long a distance as 400 mesh widths, whereas values around 0.8, were reported by Grant & Nisbet (1957) and Kistler & Vrebalovich (1966). The persistence of anisotropy in experimental situations may be influenced by large-scale non-isotropic turbulence on the upstream side of the grid. This factor, however, is not likely to have influenced the above results. The rate of return to isotropy can also depend slightly on a macroscale (i.e. integral scale) Reynolds number.

The present results indicate that the turbulence behind the grid indicate returns to a practically isotropic state within about 20 mesh widths (figure 2). The effects of tangential cooling were here accounted for in evaluating  $v_{\text{rms}}$  (see §2). For a  $k$ -value of 0.2 one would get an 8% correction for the  $v_{\text{rms}}$ -data of Comte-Bellot & Corrsin (1966), and thereby a  $v_{\text{rms}}/u_{\text{rms}}$ -ratio very close to unity. Thus, tangential cooling of the hot wires may, at least partly, explain the lack of return to isotropy behind grids reported in most earlier studies. † It is interesting to find that Batchelor & Townsend (1947) concluded in an indirect manner, from  $u$ -component measurements of the Taylor microscale, that isotropy behind a grid is reached after roughly 20 mesh widths. In figure 2  $v_{\text{rms}}/u_{\text{rms}}$  is greater than 1 close to the grid whereafter it decreases towards unity. A rapid decrease occurs in the region where the cross-stream

† Kistler & Vrebalovich used an angle calibration of their X-wire. This involved fairly large uncertainties for the determination of  $v_{\text{rms}}$  with the analogue technique used. They estimated an error limit of 10% in the wire calibrations, but this could probably be an over-optimistic value.

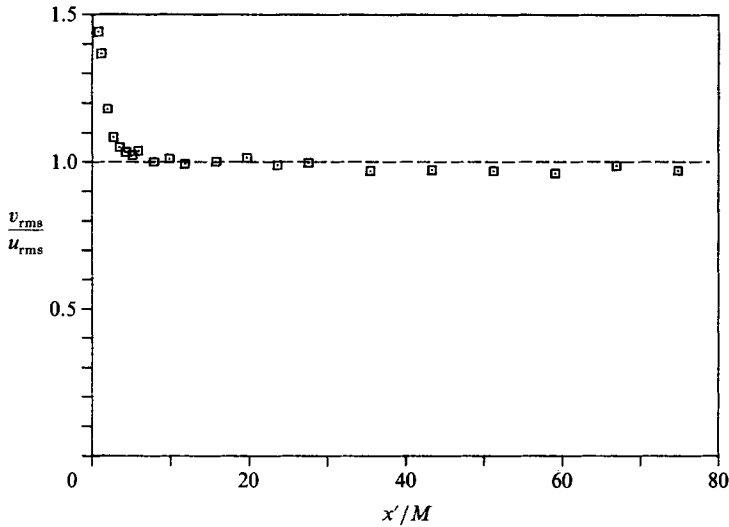


FIGURE 2. The anisotropy measure  $v_{rms}/u_{rms}$  as a function of distance downstream of the grid ( $Re_d = 2000$ ).

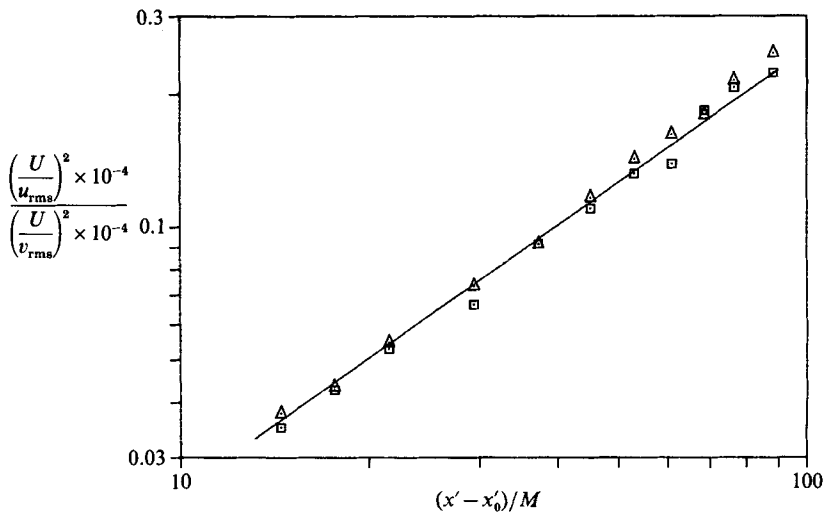


FIGURE 3. Decay of the grid turbulence.  $\square$ ,  $(U/u_{rms})^2$  and  $\triangle$ ,  $(U/v_{rms})^2$  as a function of  $(x' - x'_0)/M$ , where  $x'$  is the distance measured from the grid,  $x'_0$  is the virtual origin and  $M$  is the mesh width. The solid line represents a power-law dependence with exponent 1.0.

inhomogeneities are substantial. Beyond ten mesh widths the variation of the ratio between the intensities is very slow, and the value is typically only a few per cent below unity far downstream.

The grid-turbulence intensity  $u_{rms}$  was found to conform well to the standard type of power-law  $x$ -dependence (see Batchelor & Townsend 1948), i.e.

$$\left(\frac{U}{u_{rms}}\right)^2 = C \left(\frac{x' - x'_0}{M}\right)^n, \quad (3.1)$$

where  $x'$  is the distance downstream of the grid and  $x'_0$  is a virtual origin. Figure 3 shows the decay of turbulence intensities in the region  $x' > 20M$ , i.e. where

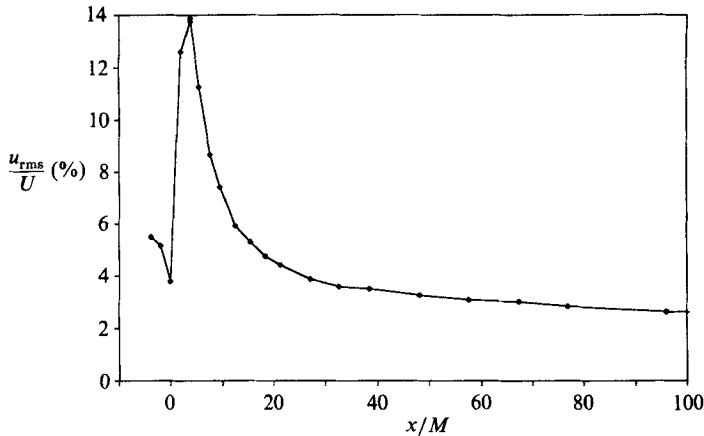


FIGURE 4. Typical example of the effect of a supercritical screen on the streamwise turbulence intensity (mesh width  $M = 0.52$  cm,  $\sigma = 0.35$  and  $Re_d \approx 330$ ).

approximate isotropy prevails. The best fit to the experimental data in this region was found for  $C = 25.2$ , a virtual origin of  $6.0M$  and an exponent  $n$  of 1.0. This is also the exponent that can be derived from simple dimensional arguments (see Tennekes & Lumley 1983). The approximate isotropy for  $x' > 20M$  implies that  $u_{rms}$  and  $v_{rms}$  obey the same decay law.

Hanarp (1981) also found a decay-law exponent, in the same region as above, of 1.0. Several other investigators (e.g. Baines & Petersen 1951; Comte-Bellot & Corrsin 1966) have found larger values of  $n$ , which can be explained by the fact that data closer to the grid have been included in the determination of the power law constants. Inclusion of data from the strongly anisotropic region leads to a larger exponent due to the more rapid decay in this region. When all data beyond  $0.8M$  were included we obtained a decay law with  $n = 1.32$ , in close agreement with the results of Wahrhaft & Lumley (1978) who obtained  $n = 1.34$  (with zero virtual origin), and with the data of Comte-Bellot & Corrsin.

The effect of a supercritical screen on the streamwise turbulence intensity ( $u_{rms}/U$ ) is illustrated in figure 4. The measurements on the upstream side were here done with the probe penetrating the screen. The turbulence intensity decreases as the flow approaches the plane of the screen due to the contraction effect and a pressure redistribution on the upstream side. Near the screen on the downstream side the turbulence intensity is higher than it would be without a screen. This is due to the vortex shedding from the wires, and the wire-wake shear layers, that give rise to high intensity small-scale turbulence, which however, decays rapidly. When only one screen is used the distance required for the intensity to fall below the incoming level was found to be about 15 mesh widths for all the supercritical screens. This distance becomes longer if the incoming turbulence level and macroscale are reduced, which is the case in screen combinations.

Figure 5(a) shows the downstream variation of the streamwise turbulence for all the screens used. All but the subcritical screen (no. 7) initially have a higher intensity than that given by the grid alone, although in this figure only data lower than the grid turbulence at  $x = 0$  are included to facilitate the comparison between the different curves. The initial decay occurs on a lengthscale determined by the mesh width, which can be seen from the collapse of the different curves when  $x$  is normalized by  $M$  (figure 5b). The mesh width seems to be a relevant lengthscale, at

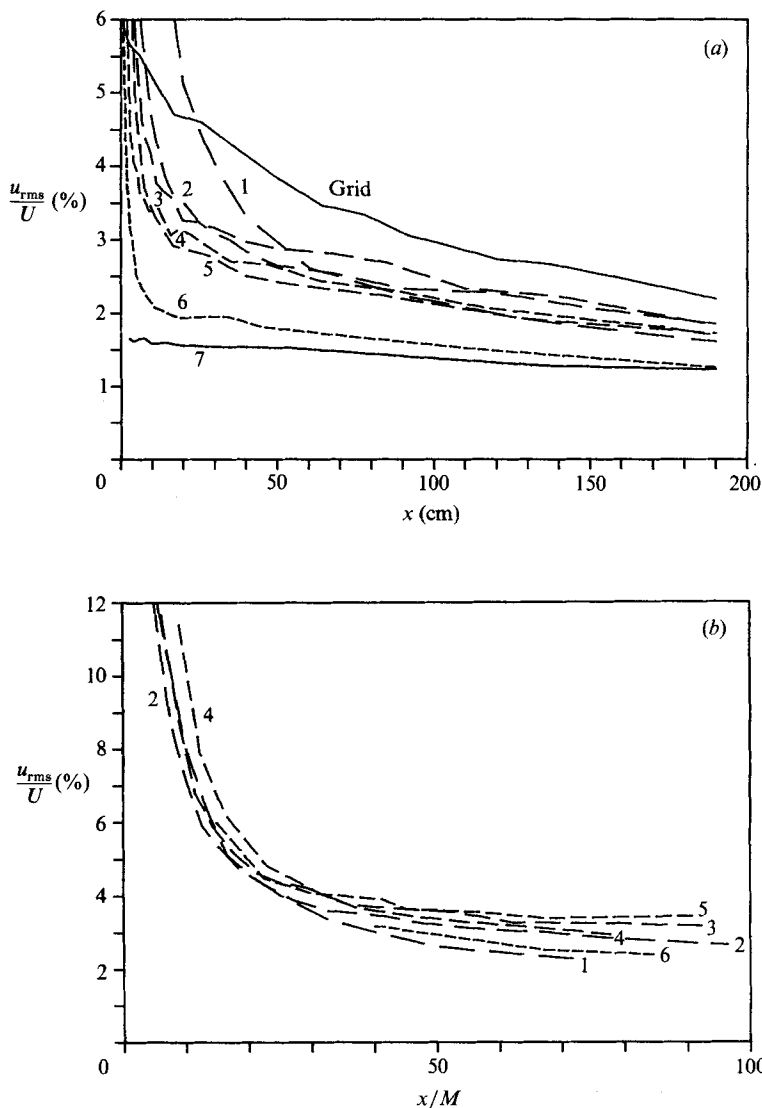


FIGURE 5.  $u_{rms}/U$  for one subcritical and six supercritical screens (numbers refer to table 1), (a) as function of  $x$  in cm and (b) as function of  $x/M$ .

least for  $x \leq 50M$ . For large  $x$ -values the rate of decay for all the screens is smaller than that for the grid (see figure 5a).

Measurements of the autocorrelation  $R_{uu}(\eta)$  where  $\eta$  is the spatial separation, computed from the temporal separation by use of Taylor's hypothesis substantiate, in an illustrative way, the predominance of small scales just downstream of a supercritical screen (figure 6a). This is manifested by the fact that both the Taylor microscale,  $\lambda$ , and the macroscale,  $A$ , at  $x = 2$  cm are much smaller (for screen no. 6 in this case) than for the grid alone. The microscale here is two mesh widths, and the macroscale is about five times larger. The ratio between the two scales is about the same for the grid alone, but here the macroscale is roughly equal to the mesh size of

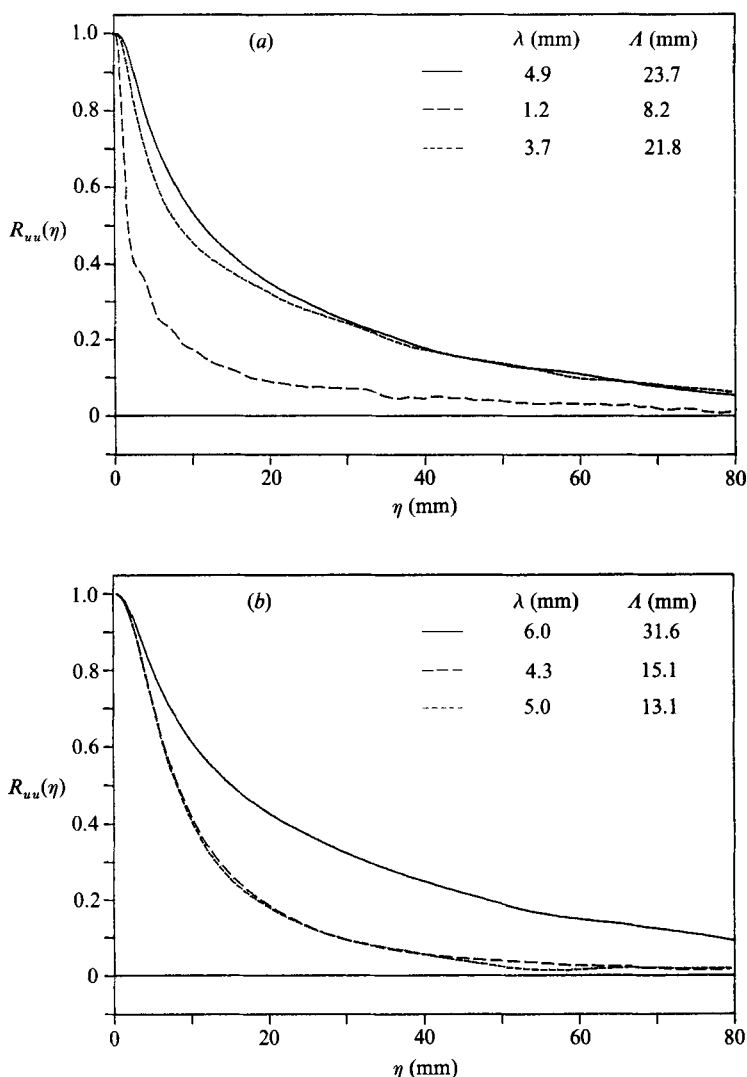


FIGURE 6. Autocorrelation functions  $R_{uu}$  for: —, the grid, ---, a supercritical screen no. 6 and - · -, a subcritical screen no. 7 at (a)  $x = 2$  cm and (b)  $x = 42$  cm.

the grid. The macroscale was determined from autocorrelations, whereas the microscale was computed from r.m.s.-values of  $u$  and its time derivative as

$$\lambda = \sqrt{2} \frac{U u_{\text{rms}}}{\left(\frac{\partial u}{\partial t}\right)_{\text{rms}}}. \quad (3.2)$$

For the subcritical screen no. 7 these scales are almost as large as for the grid alone (at  $x = 2$  cm). Although no vortex shedding occurs for the subcritical screen, fluid elements become highly stretched during the passage of the screen. The distorted turbulence exiting the screen will undergo a period of relaxation and energy transfer from the lateral components to the streamwise one. This could be seen from the

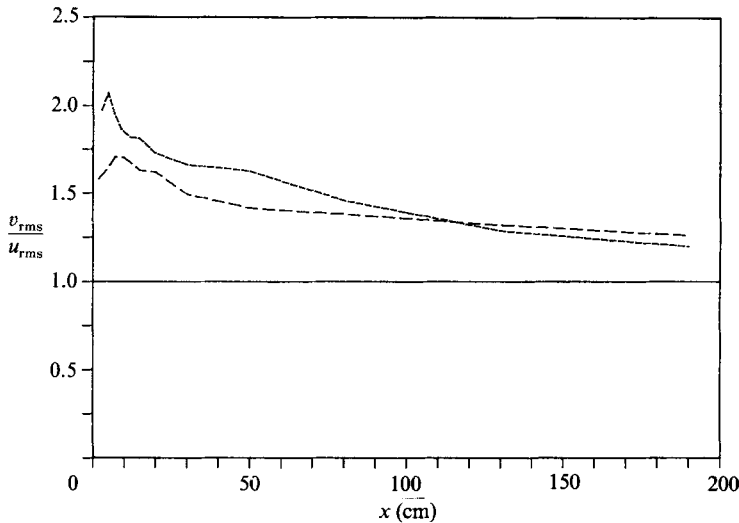


FIGURE 7. The anisotropy measure  $v_{rms}/u_{rms}$  for ---, a supercritical no. 6 and ---, a subcritical screen no. 7 as a function of  $x$ .

downstream development of the anisotropy measure  $v_{rms}/u_{rms}$  (see figure 7). The decreasing trend of  $v_{rms}/u_{rms}$  signifies an energy flux from the lateral components to the  $u$ -component, provided that the dissipation rate is about equal for all three components. One can readily find from the Reynolds-stress transport equations that, if diffusion is negligible and the dissipation tensor is isotropic, the intercomponent energy transfer to  $u_{rms}^2$  from the lateral components is proportional to the streamwise derivative of  $u_{rms}^2 - v_{rms}^2$ .

For the subcritical screen the strong energy flux from the lateral components to the streamwise component also leads to the effect that the average size of the most energetic (large-scale) turbulent eddies tends to decrease with increasing  $x$ -values for small streamwise distances. This is in contrast with isotropic decaying turbulence, and may be illustrated by the fact that the macroscale decreases by about 50% from  $x = 2$  cm to  $x = 7$  cm downstream of the subcritical screen, whereafter it increases monotonically and slowly.

Downstream of the initial rapid decay period, one may note that the energetic eddies are of considerably smaller scale for both sub- and super-critical screens as compared to those of the grid alone. This can be illustrated by the autocorrelations at  $x = 42$  cm (see figure 6*b*).

The lack of turbulence generation at the subcritical screen ensures a slow monotonic downstream development of the Taylor microscale (figure 8). Correspondingly, the fact that the turbulence behind the supercritical screen is dominated by the small scales is evidenced by a quite small microscale close to the screen, whereas the rapid decay of this part of the turbulence exhibits itself in a rapid increase of the Taylor microscale. The variation of the measured microscale downstream of the grid shows a fair agreement with that estimated theoretically under the assumption of isotropy.

In order to quantify the scales of the turbulence generated by supercritical screens power spectra were computed for various positions behind the different screens, as well as for the grid alone. The spectrum for a supercritical screen (no. 6) from the end of the initial decay region ( $x = 2$  cm or  $27M$ ) clearly yields the dominance of the

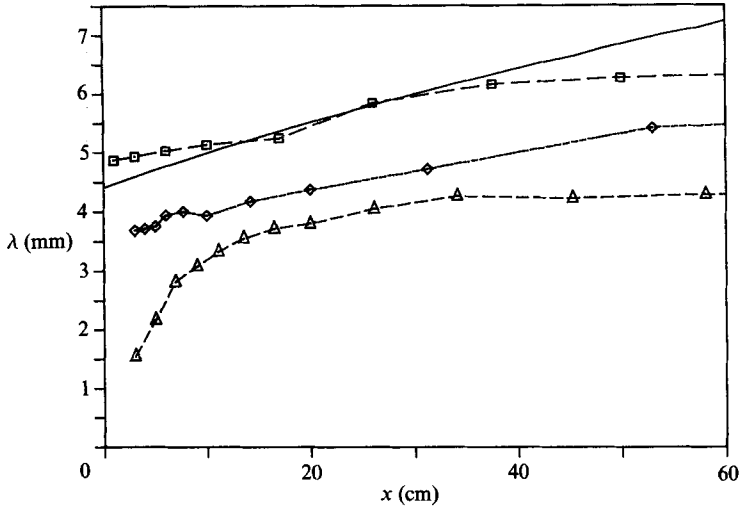


FIGURE 8. Downstream development of the Taylor microscale for  $\square$ , the grid,  $\triangle$ , a supercritical no. 6 and  $\diamond$ , a subcritical screen no. 7. The solid line represents the microscale for the grid calculated as  $\lambda^2 = 20\nu (x' - x'_0)/U$ , which can be derived from (3.1) with  $n = 1$  (under the assumption of isotropy).

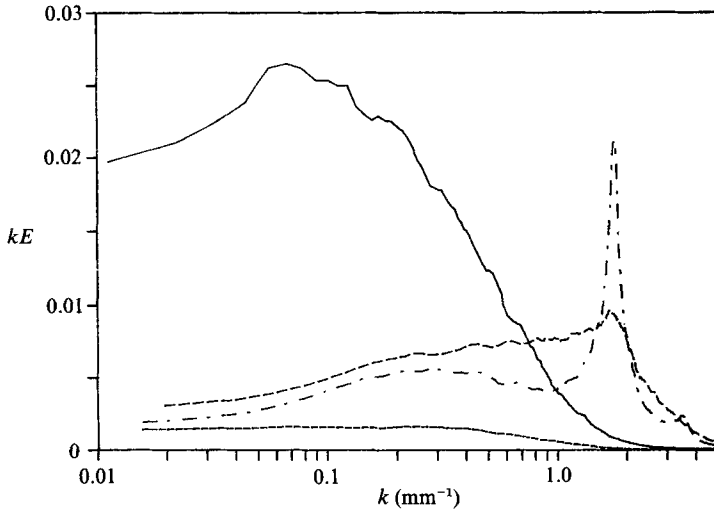


FIGURE 9. Wavenumber power spectra at  $x = 2$  cm, for —, the grid, ---, a supercritical no. 6, ---, a subcritical screen no. 7 and ···, a combination of two screens no. 6 with 10 cm separation. The spectra are shown in absolute scale, i.e. the area under each curve is equal to  $u_{rms}^2$ .

generated small-scale turbulence, and a strong suppression of the large scales (figure 9). In absolute terms the energy is reduced by a factor of three for wavenumbers corresponding to the incoming macroscale, whereas above  $0.8 \text{ mm}^{-1}$  the energy is increased by a maximum one order of magnitude. A sharp peak is seen at wavenumbers around  $1.7 \text{ mm}^{-1}$ , or equivalently, at wavelengths of about 5 mesh widths or 20 wire diameters. However, neither of these numbers was found to be universal, i.e. the same for different screens. Instead, the appropriate scaling involves both quantities mentioned. The width of this power spectral peak was found to increase with increasing wire-diameter Reynolds number, as should be expected. The

position of the high wavenumber peak was found to be independent of the incoming turbulence. This could be concluded from spectral measurements behind two screens in which case the incoming turbulence to the downstream screen is significantly different in scale from that to a single screen. For comparison the spectrum at  $x = 2$  cm for the subcritical screen is also included in figure 9, and shows only a moderate change in the wavenumber energy distribution as compared with the grid alone. This is in accordance with the micro- and macro-scale data (figure 6).

To study the development of the dominant high wavenumber peak, spectra were measured in the immediate vicinity of a fairly coarse screen through which the hot wire could be protruded. A comparison between a position one mesh width upstream and one in the plane of the screen showed that the maximum in the incoming power spectrum was shifted towards lower wavenumbers, roughly by a factor of 0.5, reflecting the stretching of fluid elements. At one mesh width downstream, the broad peak corresponding to the maximum at  $x = 0$  could still be clearly seen, but now accompanied by a high wavenumber peak from the screen-generated turbulence. From  $x = 2M$  and throughout the initial decay region the spectrum is dominated by the screen-generated turbulence, although the peak is slowly moved towards lower wavenumbers due to the influence of dissipation.

Both sub- and super-critical screens reduce the streamwise turbulence intensity more effectively than the lateral ones, in agreement with the analysis of Taylor & Batchelor (1949). The ability to reduce the streamwise intensity increases, for a given solidity, with decreasing mesh size (see figure 5*a*), but the same trend is weaker for  $v_{\text{rms}}$ , which results in a strong anisotropy downstream of fine mesh screens. For the subcritical screen  $v_{\text{rms}}/u_{\text{rms}}$  had a maximum value of about 2.1 (figure 7), which implies, since the lateral components are of nearly equal intensity, that 90% of the energy was contained in the lateral components.

For both types of screens the return to isotropy was found to be very slow, and take place on a lengthscale that is substantially larger than that for the unmanipulated grid turbulence. The latter returned to approximate isotropy within 20 mesh widths (i.e. 50 cm), whereas the flow behind the screens did not quite reach isotropy within the 2 m long test section. This may seem surprising, but can be understood from the following reasoning. The turbulent kinetic energy,  $q$ , decays on a lengthscale which can be estimated as  $L_{\text{decay}} = q/(-dq/dx)$ . From the Reynolds-stress transport equations (see e.g. Launder, Reece & Rodi 1975) one can show that the return to isotropy occurs on a lengthscale  $L = qU/\epsilon$ , where  $\epsilon$  is the rate of dissipation. This return is caused by the pressure-strain correlation terms (see Rotta 1951). Under the assumption of Taylor's hypothesis the lengthscales  $L$  and  $L_{\text{decay}}$  are identical.  $L_{\text{decay}}$  was computed from the variation of the turbulent energy, and it was found to be typically a factor of five larger (in the region 0.1–0.5 m) for the supercritical screen (no. 6) than that for the grid. This together with the initial high degree of anisotropy behind the screens explains the large distance required for the return to isotropy.

The larger  $L_{\text{decay}}$  for the flow behind screens reflects a smaller rate of dissipation than for the grid alone. For isotropic turbulence  $\epsilon$  can be expressed as

$$\epsilon = 30\nu \frac{u_{\text{rms}}^2}{\lambda^2} \quad (3.3)$$

This relation indicates the qualitative dependence of  $\epsilon$  on turbulence intensity and microscale even for anisotropic cases. The smaller dissipation downstream of screens,

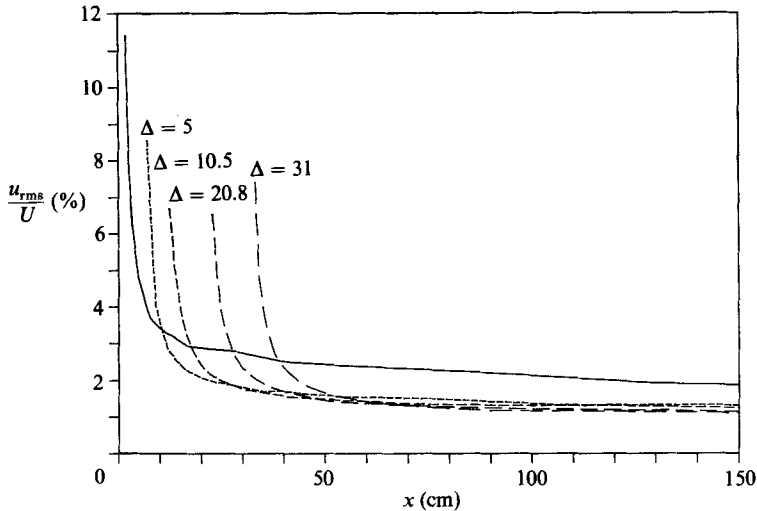


FIGURE 10. The development of  $u_{rms}/U$  downstream: —, one screen no. 4 with  $Re_a \approx 170$  and ---, a combination of two such screens with various separations,  $\Delta$  (in cm).

as compared with that for the grid, is coupled to a strong reduction in intensities while the microscale is only moderately affected (see figures 5*a* and 8).

### 3.1. Screen combinations

When screens are used in combination their separation should at least correspond to the length of the initial decay region. Figure 10 shows the turbulence intensity downstream of a pair of supercritical screens (no. 4) for various separations between 25 and 150 mesh widths. The former roughly corresponds to the length of the initial decay region (see figure 5*b*). The total reduction depends only slightly on the separation within this range. It may here be worth mentioning that Dryden & Schubauer (1947) found no effect of varying the spacing (from 5 to 70 cm) between the screens in a wind-tunnel stagnation chamber when the measurements were carried out in the test section.

One may, rather arbitrarily, construct a reduction factor as the ratio between the incoming intensity and that far, say 1 m, downstream of a screen. This would give a reduction factor of 2.9 for a single screen (no. 4), whereas a combination of two gives a total reduction factor of 4.8. The downstream screen, which encounters a more 'fine-grained' turbulence with lower intensities, hence gives a smaller turbulence reduction.

For a given allowable pressure drop the amount of turbulence reduction obtained depends strongly on mesh sizes, and on how different types of screens are combined, as is illustrated in figures 11 (*a*, *b*) for two-screen combinations. Firstly, it is seen that a combination of two different supercritical screens, the coarsest being the upstream one, gives a substantially greater reduction than a subcritical screen alone (figure 11*a*), although the  $K$ -values for the combination and the subcritical screen are approximately equal. Hence, although subcritical screens give high reduction factors, their penalty in terms of pressure drop makes them undesirable for practical purposes. For wind-tunnel applications they also have the disadvantage of being prone to clogging by small dust particles.

A cascade combination (see figure 11*b*) gives a slightly larger reduction, for moderate  $x$ -values, than if the coarser screen were to be replaced by one more of the

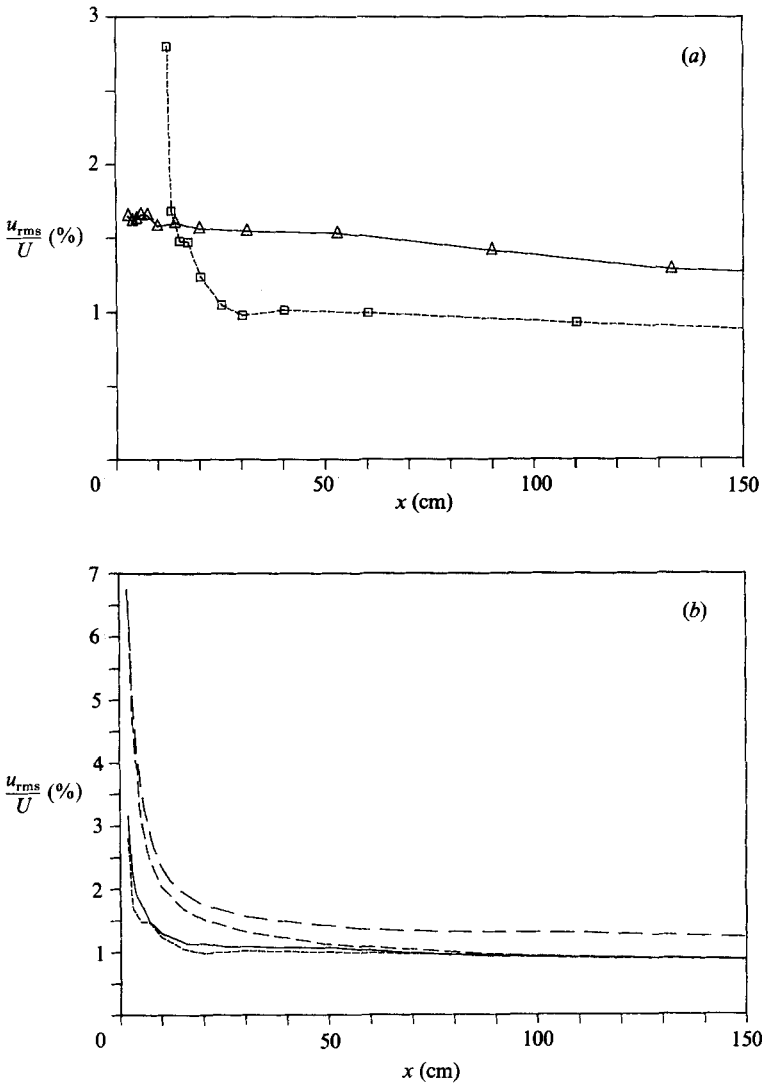


FIGURE 11.  $u_{rms}/U$  downstream of two-screen combinations, all with 10 cm separation. (a) Comparison between  $\square$ , a cascade combination of supercritical screens (no. 4+no. 6) and  $\Delta$ , a single subcritical screen no. 7.  $K = 2.7$  for both cases. (b) Comparison between ---, the no. 4+no. 6 and - · - ·, a reversed cascade combination no. 6+no. 4. Included are also — — no. 4+no. 4 and —, no. 6+no. 6.

finer type, although the latter combination has a 25% higher  $K$ -value. A reversed cascade combination of the same screens gives higher turbulence intensities over a long region in the streamwise direction, which makes them unsuitable for use in wind-tunnels. However, far downstream the intensity level becomes, somewhat surprisingly, equal to that of the regular cascade combination. As should be expected, two coarse screens give less reduction than either type of cascade, for all  $x$ -values.

The streamwise turbulence intensity was measured behind various two-screen cascade combinations with a fine-mesh supercritical screen (no. 6) as the downstream one. A constant separation of 10.5 cm was used, which corresponds to more than 20

mesh widths for all cases. This allows for the initial period of rapid decay to take place upstream of the second screen. The damping varied fairly little between different combinations although  $Re_d$  of the upstream screen varied between 65 and 330. This is interesting since it allows a given turbulence reduction to be achieved for quite different pressure drops. The typical lengthscales generated by each screen in a combination should be substantially smaller than the incoming macroscale, but aside from this the damping ability of the combination is relatively insensitive to the specific lengthscale ratio and total pressure drop.

Dryden & Schubauer (1947) gives an empirical formula for the turbulence damping by screen combinations. The damping is calculated as the product of factors  $(1 + K_i)^{0.5}$  ( $i = 1, N$ ), where  $K_i$  is the respective  $K$ -value and  $N$  is the number of screens. This would imply an approximately 25% lower turbulence intensity behind the no. 6 + no. 6 combination as compared to the no. 2 + no. 6 case, while measurements showed almost equal levels. The latter combination has a pressure drop coefficient which is only two thirds of that for the former. One should here remember that the dissipation obscures the generality of conclusions about reduction factors, and makes comparisons with formulae, such as the one just described, rather doubtful.

Various three-screen combinations were tested and the lowest turbulence level at  $x = 1$  m was 0.78% (to be compared with the incoming level of 5.5%), which was obtained for a typical cascade combination (no. 3 + no. 4 + no. 6). This was further complemented with one each of the two finder screens resulting in a total  $K$ -value of 5.8, and a total intensity reduction factor of about 12 (defined as above). The formula given by Dryden & Schubauer (1947) would give a value of 6.4 for this five-screen combination.

#### 4. Summary and conclusions

Turbulence generated by a (biplane square rod) grid was found to undergo a transition to approximate isotropy from the initially strongly anisotropic state within a region roughly 20 mesh widths long. The persistent anisotropic character far downstream of the grid as found by some earlier investigators, can partly be explained by influence of tangential cooling of the hot wires used. This part of the heat loss from the wires acts to reduce the apparent intensity of the lateral component (see (2.3)). In the approximately isotropic region ( $x' > 20M$ ) the kinetic energy, and  $u_{\text{rms}}^2$ , were found to obey a 'linear decay law', i.e. with an exponent of 1.0. This exponent increased if parts of, or the whole, anisotropic region were included. This explains the discrepancies reported in the literature regarding the decay law exponent.

The pressure drop coefficient for screens was found to conform well to the general form (equation (2.1)) given by Pinker & Herbert (1967) where the dependence on solidity is given and the wire diameter Reynolds number enters in a multiplicative function  $f$ . The asymptotic value of  $f$  for high Reynolds numbers,  $Re_d > 300$ , was here found to be approximately 0.45, which is somewhat lower than that found by Pinker & Herbert.

The turbulence damping ability of a screen increases with decreasing mesh size for a given solidity. Subcritical screens thus give a large turbulence reduction, but their 'penalty' in terms of a high pressure drop makes them inferior for practical use as compared with cascade combinations of supercritical screens. Also, at the velocities

typically used in the stagnation chamber in the middle to upper velocity range in a low-speed tunnel ( $\sim 5$  m/s) very small wire-diameters are needed for screens to be subcritical (0.040 mm was used in the present case), which makes them susceptible to dirt contamination (and expensive).

The flow in the region immediately downstream of a supercritical screen has a distinctly different character from that far downstream. Both regions were found to exhibit several interesting features that differ from those of the unmanipulated flow. In the immediate vicinity of the screen the turbulence intensities are substantially higher than on the upstream side. The energy spectrum is dominated by the screen-generated turbulence, and the dominating wavelengths are a few mesh widths independent of the scale of the incoming turbulence. Within the first 15–25 mesh widths, ‘the initial decay region’, the intensities decrease rapidly, and for a single screen fall below the incoming levels. The dominating spectral peak was found to persist throughout this region, but is slowly shifted towards lower wavenumbers due to the influence of dissipation. The increase in energy for small scales is contrasted by a strong suppression of the low wavenumber regime. Within the initial decay region the turbulence was found to be strongly anisotropic for both sub- and supercritical screens, causing an energy transfer from the lateral to the streamwise component. This was most clearly seen for subcritical screens, for which the maximum anisotropy corresponded to a situation with 90% of the energy in the lateral components. Both types of screens exhibit a much slower return to isotropy than the grid. This was shown to be consistent with a larger lengthscale of decay beyond the initial decay region. Hence, the anisotropic character behind screens persists into the ‘far-field region’, which also is characterized by a smaller rate of decay than for the grid alone.

When screens are used in combination their separation should be chosen larger than the length of the initial decay region. As long as this criterion is satisfied the separation only slightly affects the damping. For a given total pressure drop the maximum turbulence reduction was found for cascade type of screen combinations where the last screen (in the streamwise direction) was chosen with a low, albeit supercritical, Reynolds number. This ensures small scales produced by the last screen and thereby a short initial decay region. To minimize the pressure drop the other screens should be chosen with increasing mesh size in the upstream direction. The pressure drop decreases with increasing Reynolds number (for a given solidity) for  $Re_d < 300$ , but levels off above this value, which hence may serve as a guide for choosing the coarsest screen.

A combination of a relatively coarse screen followed by a finer one gave at least as effective a turbulence reduction as a pair of the finer type of screen, although the latter had a considerably higher pressure drop coefficient. This invalidates any quantitative description of damping solely based on screen properties such as the pressure drop coefficient. Experiments with two-screen combinations also showed that the damping ability depends only slightly on the typical lengthscale (e.g. the macroscale) of the incoming turbulence, at least as long as this scale was substantially larger than the mesh size.

As an illustration of the reduction achievable with cascade screen combinations realistic for application in low-speed wind tunnels, it may be mentioned that a set of five screens, with  $Re_d$  from 170 down to 65, was found to give a total reduction, 1 m downstream of the last screen, of a factor 12 compared with the incoming intensity.

We wish to thank Professor Henrik Alfredsson for actively taking part in the construction of the wind tunnel, and for many helpful comments, and Magnus Hallbäck for assisting with some of the measurements. Support from the Swedish Board for Technical Development is gratefully acknowledged.

## REFERENCES

- BAINES, W.D. & PETERSEN, E. G. 1951 An investigation of flow through screens. *Trans. ASME* **73**, 467–480.
- BATCHELOR, G. K. 1976 *The Theory of Homogeneous Turbulence*, chapter 4. Cambridge University Press.
- BATCHELOR, G. K. & TOWNSEND, A. A. 1947 Decay of vorticity in isotropic turbulence. *Proc. R. Soc. Lond. A* **190**, 534–550.
- BATCHELOR, G. K. & TOWNSEND, A. A. 1948 Decay of isotropic turbulence in the initial period. *Proc. R. Soc. Lond. A* **193**, 539–558.
- CHAMPAGNE, F. H., SLEICHER, C.A. & WEHRMANN, O. H. 1967 Turbulence measurements with inclined hot-wires. *J. Fluid Mech.* **28**, 153–182.
- COMTE-BELLOT, G. & CORRSIN, S. 1966 The use of a contraction to improve the isotropy of grid-generated turbulence. *J. Fluid Mech.* **25**, 657–682.
- CORRSIN, S. 1963 *Turbulence: Experimental Methods. Handbuch der Physik*, vol. 8, part 2, pp. 524–590. Springer.
- DRYDEN, H. L. & SCHUBAUER, G. G. 1947 The use of damping screens for the reduction of wind-tunnel turbulence. *J. Aero. Sci.* **14**, 221–228.
- GRANT, H. L. & NISBET, I. C. T. 1957 The inhomogeneity of grid turbulence. *J. Fluid Mech.* **2**, 263–272.
- HANARP, L. 1981 An experimental study of grid-generated freestream turbulence and its influence on velocity and temperature boundary layers on circular cylinders. PhD thesis, Dept of Applied Thermo and Fluid Dynamics, Chalmers University of Technology, Göteborg, Sweden.
- HINZE, J. O. 1959 *Turbulence*, chapters 2.4, 3 and 4. McGraw-Hill.
- KISTLER, A. L. & VREBALOVICH, T. 1966 Grid turbulence at large Reynolds numbers. *J. Fluid Mech.* **26**, 37–47.
- LAUNDER, B. E., REECE, G. J. & RODI, W. 1975 Progress in the development of a Reynolds-stress turbulence closure. *J. Fluid Mech.* **68**, 537–566.
- LAWS, E. M. & LIVESEY, J. L. 1978 Flow through screens. *Ann. Rev. Fluid Mech.* **10**, 247–266.
- PINKER, R. A. & HERBERT, M. V. 1967 Pressure loss associated with compressible flow through square-mesh wire gauzes. *J. Mech. Engng Sci.* **9**, 11–23.
- PRANDTL, L. 1932 Herstellung einwandfreier Lufströme (Windkanäle). *Handbuch der Experimentalphysik*, Leipzig, Germany, vol 4, part 2, p. 73. *NACA Tech. Mem.* 726.
- ROTTA, J. C. 1951 Statistische Theori nichthomogener Turbulenz. *Z. Phys.* **129**, 547–572.
- SCHUBAUER, G. G., SPANGENBERG, W. G. & KLEBANOFF, P. S. 1950 Aerodynamic characteristics of damping screens. *NACA Tech. Note* 2001.
- TAN-ATICHAT, J., NAGIB, H. M. & LOEHRKE, R. I. 1982 Interaction of free-stream turbulence with screens and grids; a balance between turbulence scales. *J. Fluid Mech.* **114**, 501–528.
- TAYLOR, G. I. & BATCHELOR, G. K. 1949 The effect of wire gauze on small disturbances in a uniform tream. *Q. J. Mech. Appl. Maths* **2**, 1–29.
- TAYLOR, G. I. & DAVIES, R. M. 1944 The aerodynamics of porous sheets. *Aero. Res. Council. R & M* 2237.
- TENNEKES, H. & LUMLEY, J. L. 1983 *A First Course in Turbulence*, chapter 3.2. The MIT Press.
- WAHRHAFT, Z. & LUMLEY, J. L. 1978 An experimental study of the decay of temperature fluctuations in grid-generated turbulence. *J. Fluid Mech.* **88**, 659–684.